Cleaner Materials 12 (2024) 100240

Contents lists available at ScienceDirect

Cleaner Materials

journal homepage: www.journals.elsevier.com/cleaner-materials

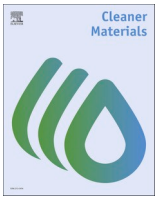

Green engineered cementitious composites with enhanced tensile and flexural properties at elevated temperatures

S. Rawat [a,b], C.K. Lee [b], Y.X. Zhang [a,*]

[a] School of Engineering, Design and Built Environment, Western Sydney University, NSW 2751, Australia
[b] School of Engineering and Technology, The University of New South Wales, Canberra, ACT 2600, Australia

ARTICLE INFO

Keywords:
Engineered cementitious composite
Elevated temperature
Green construction material
Polyethylene fibre
Residual strength

ABSTRACT

This study provides new insights in the design of green hybrid polyethylene (PE)-steel fibre reinforced high strength engineered cementitious composite (HSECC) with superior tensile and flexural strength at both ambient and elevated temperatures. Blends of high volume of ground granulated blast furnace slag (GGBFS), dolomite powder and fly ash were utilized to achieve a 60 % cement replacement for the HSECC mixes. These mixes were then exposed to 20–600 °C and a total of 210 specimens were tested to assess their residual tensile stress–strain behaviour, flexural load–displacement response, and toughness. Results indicate that high volume of GGBFS can be very effective in limiting the surface damage and retaining high strength at elevated temperatures. A combination of 1.5 % PE-0.75 % steel with quaternary blend of GGBFS, dolomite and fly ash demonstrated at least 60 % and 40 % retention in tensile and flexural strength at 600 °C, respectively. This was significantly better than the strength of the traditional control silica fume mix considered in this study as well as results reported in many previous literatures on HSECC. Microstructural examination was further conducted to understand the mechanism of fibre deterioration and justify the resulting change in pseudo-hardening behaviour with temperature rise. Findings obtained in this study clearly demonstrated the effectiveness of PE-steel fibre hybridisation at elevated temperature and confirmed that with right binder selection, superior tensile and flexural performance can be achieved even with a very high cement replacement level.

1. Introduction

Engineering cementitious composite (ECC) is a class of high-performance fibre reinforced cementitious composites having superior tensile performance with strain capacity as high as 12.5 % (Zhang et al., 2019). The unique mechanical properties such as high tensile ductility can be achieved by using fibres via tailoring fibre matrix interaction appropriately. In general, ordinary Portland cement and silica sand are the most commonly used ingredients in conventional ECC (Shoji et al., 2022), and the manufacturing of both the constituents is energy intensive. Moreover, the amount of cement used in ECC is significantly higher than that used in normal concrete due to the absence of coarse aggregates. Not only has this led to environmental concerns because of the substantial carbon emissions linked to cement manufacturing, but it has also possibly increased durability issues such as autogenous shrinkage due to the high volume of cementitious paste (Lai et al., 2021). Researchers have been making continuous efforts in recent years to make ECC greener by using various types of supplementary cementitious materials (SCMs) or industry by-products such as fly ash (FA), silica fume, limestone calcined clay blends, and ground granulated blast furnace slag (GGBFS), and waste glass powder. These SCMs are either utilized as partial substitutes for ordinary Portland cement (OPC) (Zhang et al., 2021; Tosun-Felekoğlu et al., 2017; Zhang et al., 2020; Deng et al., 2022; Hou et al., 2022; Yu et al., 2020) or activated using alkalis to eliminate the need for OPC (Lao et al., 2022; Lao et al., 2023). Moreover, the problem of autogenous shrinkage has also been found to reduce with the use of the high volume of SCMs such as FA, GGBFS (Lai et al., 2021; Lai et al., 2022; Yang et al., 2024).

While FA has been traditionally used as primary SCM in ECC (Shoji et al., 2022), there is a shift towards the use of alternative materials like GGBFS due to concerns over the declining supply of FA from coal plants. GGBFS, a by-product obtained of iron production, is gaining attraction due to its established benefits in concrete including superior mechanical and durability properties (Amran et al., 2021). Moreover, concrete with GGBFS has also shown better performance than fly ash and silica fume under elevated temperatures (Sullivan and Sharshar, 1992). Dolomite

* Corresponding author.
E-mail address: sarah.zhang@westernsydney.edu.au (Y.X. Zhang).

https://doi.org/10.1016/j.clema.2024.100240
Received 25 January 2024; Received in revised form 25 February 2024; Accepted 16 March 2024
Available online 18 March 2024

powder, derived from carbonate rocks, is emerging as another promising material. Waste powder containing dolomite sourced from stone quarries has been proven to be effective in enhancing the compressive strength of concrete (Mikhailova et al., 2013). Furthermore, dolomite has a unique composition containing 47 % CO_2 and thus may be particularly effective in improving fire resistance. Recently, authors proposed an optimized mix for a new type of ECC utilizing both dolomite powder and high volume of GGBFS with a total 60 % cement replacement (Rawat et al., 2022). The developed ECC demonstrated excellent mechanical performance further confirming the suitability of use of GGBFS and dolomite powder in ECC.

With the increased focus on the utilization of such alternative binder materials, it also becomes critical to analyse its behaviour at elevated temperatures. Elevated temperature resistance is particularly important for ECC due to its denser microstructure which could increase the risk of spalling and may also lead to reduced residual performance. Currently, there is a lack of conclusive findings on the elevated temperature behaviour of fibre reinforced cementitious composites especially for polyethylene (PE) fibre reinforced ECC (PE-ECC) (Rawat et al., 2021). Existing studies have not only reported poor spalling resistance for PE-ECC but have also observed a sharp decline in the tensile or flexural strength. Liu et al. (Liu and Tan, 2018) reported that ultra-high-performance strain hardening cementitious composites were prone to spalling when reinforced solely with 1.3 % (by vol.) PE fibres. Additionally, while the use of hybrid PE (1.3 %) and steel (1 %) fibre prevented spalling, a significant loss in tensile strength occurred, with 71 % reduction at 600 °C. Zhang et al. (Zhang et al., 2021) observed explosive spalling in specimens containing only 1.5 % PE fibre. However, the specimens with hybrid PE and polypropylene fibre (0.3–0.5 %) were able to resist spalling and retained around 25–38 % strength at 800 °C. Li et al. (Li et al., 2020) also reported spalling and significant performance deterioration in prism specimens with hybrid steel (2 %) and PE (1 %) fibre at 600 °C. Overall, existing literature show that PE fibre reinforced ECC demonstrate poor spalling resistance and inferior tensile or flexural performance after elevated temperature exposure. Hybrid fibre combination of PE with PP or steel fibres may be promising to develop fire resistant ECC, however, the research in this area is still very limited to establish a conclusive trend. Since ECC is primarily characterized by its high tensile or flexural performance, it is imperative to thoroughly investigate its behaviour under elevated temperature conditions to broaden its practical applications.

In addition to the fibres, matrix constituents also play significant role in post-fire strength retention of ECC. It is important to note that previous studies have predominantly employed silica fume as the primary binder material, which itself has a high probability of spalling (Rawat et al., 2021). The post-cracking tensile or flexural performance of ECC are governed by fibre bridging which in turn is dependent on fibre type and fibre matrix interface. Hence, analysing the effect of different matrix constituents and fibre proportions is critical in understanding the mechanism of ECC at elevated temperatures.

Therefore, this paper addresses these gaps by systematically investigating the effect of binder material on the residual tensile and flexural performance of hybrid PE-steel fibre reinforced high strength ECC (HSECC) at elevated temperatures (ranging from 200 to 600 °C). The blend of GGBFS, fly ash and dolomite developed in the authors' recent study (Rawat et al., 2022) was adopted as main mix due to its high potential to resist thermal attack and reduced dependence on cement. Hybrid combination of PE and steel fibres was specifically used to reduce the risk of spalling and understand the synergy of hybrid fibres on residual performance. Dosages of binder material and fibres were further varied within the recommended range (Rawat et al., 2022) to analyse the effect of binder material on the residual tensile and flexural performance of the HSECC. Additionally, the performance of this hybrid mix was compared with an HSECC mix containing silica fume as the primary SCM, aiming to comprehensively investigate the influence of various binder systems. Scanning electron microscopic (SEM) analysis was also used to study the states of fibres and microcracks development in HSECC matrix against elevated temperature exposure.

2. Experimental programs

2.1. Materials

Different blends of four types of SCMs including GGBFS, fly ash, dolomite powder, and silica fume (Fig. 1) were used to study the effect of the binder material on the residual performance of the mixes. General-purpose cement, Class F FA and GGBFS were supplied by Boral, Australia. Fly ash used was class F type with > 87 % passing through 45 μm. The specific surface area of GGBFS used was 445 m^2/kg. The densified silica fume and dolomite were procured from Synergy Pigments, Australia and Tianjin Yandong Mining Co. Ltd., China respectively. Both materials had a particle size finer than 45 μm, with over 95 % passing through the sieve. More details about the material composition can be found in the authors' previous work (Rawat et al., 2022). Apart from the other common ingredients such as cement, high range water reducer (HRWR) and water, local river sand passing through 300 μm sieve was utilized as fine aggregate. This substitution for traditional silica sand was aimed to achieve a balance between cost-effectiveness and structural suitability (Meng et al., 2017). Additionally, hybrid combination of PE fibres (length 12 mm, diameter 24 μm) and steel fibres (length 13 mm, diameter 200 μm) was utilized, where steel fibres were added to enhance the cracking strength and PE fibres were utilized to impart superior tensile ductility and spalling resistance.

2.2. Mix designs

Five distinct types of mixes (M1-M5) with constant water-binder ratio of 0.2 were considered in the present study as highlighted in Table 1. Mix M1 is the optimal mix which was developed in the authors' previous work using integrated Taguchi method based multi response optimization (Rawat et al., 2022). 60 % (by weight) of cement was replaced by the SCM in this mix with GGBFS:FA ratio = 1:0.2 and dolomite powder as 15 % of the binder weight. This mix satisfied the structural performance requirement in terms of its mechanical performance, and also showed superior residual compressive performance at high heating rate and in-situ conditions (Rawat et al., 2022; Rawat et al., 2024). The content of dolomite was reduced to 10 % of the binder weight in mix M2 to analyse the residual effect of dolomite powder. Mix M4 only had GGBFS with cement to GGBFS ratio 1:1 (50 % replacement) and this was mainly done to evaluate the feasibility of GGBFS based HSECC at both room and elevated temperatures. Furthermore, since silica fume is the most commonly used SCM in PE fibre reinforced ECC, mix M5 was specifically considered to analyse the effect of type of matrix constituent. This mix was adopted from Zhang et al. (Zhang et al., 2021) and uses only cement and silica fume as the main binders. Mixes M1, M2, M4 and M5 were all formulated with 1.5 % PE fibre and 0.75 % steel fibre volume. To study the effect of fibre content on the residual tensile and flexural performance, volume of PE and steel fibres was changed from 1.5 to 1.25 % and 0.75 to 1 % respectively in mix M3. All mixes showed remarkably high 56-day compressive strength ranging from 138.1 to 153.7 MPa (Table 1) satisfying the criteria of terming the developed mixes as HSECC.

1.3. Specimen preparation and heat treatment

Firstly, dog-bone specimens of size 368 mm × 80 mm × 20 mm for tensile test and prismatic specimens of size 50 mm × 50 mm × 350 mm (300 mm effective span) for flexural test were cast using the procedure stated in Khan et al. (Khan et al., 2020) and were cured at standard curing condition in fog room (23 ± 1 °C and 95 ± 5 % relative humidity) for 28 days. At the end of the standard curing period, the samples were kept in an environmental room at 20 °C and 55 % relative humidity for

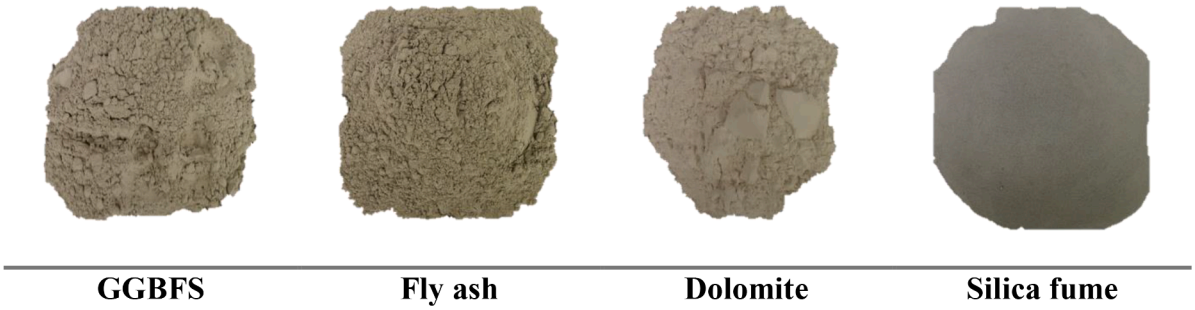

Fig. 1. SCMs used in the present study.

Table 1
Mix proportions used in this study.

Mix ID	Binder				Sand	Water	HRWR	PE	Steel	
	Cement	GGBFS	FA	Dolomite						56-days compressive strength (MPa)
M1	1	0.94	0.19	0.38	0.91	0.50	0.05	1.50 %	0.75 %	138.1
M2	1	0.83	0.17	0.22	0.81	0.44	0.04	1.50 %	0.75 %	142.4
M3	1	0.94	0.19	0.38	0.91	0.50	0.05	1.25 %	1 %	145.2
M4	1	1.00	0.00	0.00	0.73	0.40	0.04	1.50 %	0.75 %	143.7
Mix ID	**Cement**	**Silica fume**	**FA**	**Dolomite**	**Sand**	**Water**	**HRWR**	**PE**	**Steel**	
M5	1	0.11	0.00	0.00	0.44	0.22	0.02	1.50 %	0.75 %	153.7

Note: Fibre content is expressed in volume fraction of the mix, whereas all other constituents' ratios are expressed as weight proportion of the cement content. Compressive strength is calculated for 75 mm diameter × 150 mm height cylinders under the same curing conditions as followed in this paper.

another 28 days to remove any excess moisture. Thereafter, the specimens were placed in the furnace and exposed to 200, 300, 400, 500, and 600 °C at 1 °C/min. A slow heating rate was chosen to prevent damage from large thermal gradients, allowing for effective study of material properties. It should be noted that despite the slow heating rate, variations in temperature distribution may occur between the surface and core of the specimens depending on the material and testing conditions (Lai et al., 2024; Ho et al., 2022; Zhuang et al., 2022). Therefore, after reaching the target temperature, a dwell period of 2 h was implemented to ensure an isothermal state. This duration has been found sufficient in previous studies (Zhang et al., 2021; Tangirala et al., 2023). After the completion of heating, the specimens were allowed to cool by turning off the furnace until the ambient temperature was reached. For each set of mix and temperature, four specimens were tested for tension and three specimens were tested for flexure (summing to a total of 210 specimens) to consider the average effect. The general notation used to denote the specimen is 'MX-T' where MX is the mix ID with X = 1…5 and T is the exposure temperature ranging from 20 to 600 °C. For instance, M1-400 represents M1 mix specimens which first underwent 400 °C exposure and were naturally cooled.

2.4. Tensile and flexural tests

Tensile testing was performed on a 100 kN capacity Shimadzu AG-X machine at a loading rate of 0.1 mm/min to assess the residual tensile stress–strain behaviour of the HSECC mixes. Two targets were glued at the end of gauge length on both side of the specimen (Fig. 2a) and their relative movement was captured by a pair of Shimadzu TRViewX non-contact digital extensometers to measure the elongation. Ultimate tensile strain is considered to be at the point when the load has dropped to 75 % of its maximum value as recommended by Khan et al. (Khan et al., 2020) for hybrid ECC. Four-point bending tests were also conducted using the same machine in accordance with standard ASTM C1609 (Astm c1609, 2019) to evaluate the flexural load–displacement response of the HSECC specimens. The prismatic specimens were tested under a displacement control condition at a loading rate of 0.05 mm/min. The setup used was similar as that in the uniaxial tensile strength test with two targets, one glued at the bottom of the beam (Fig. 2b) with other kept fixed and their relative movement was captured by a pair of Shimadzu TRViewX non-contact digital extensometers. A digital single lens reflex camera was also used to record images for digital image correlation (DIC) analysis.

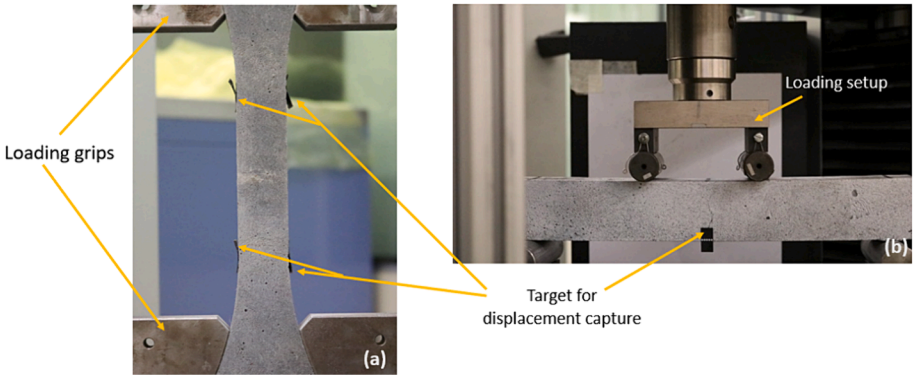

Fig. 2. Set up for (a) tensile test; (b) four-point bending test.

3. Results and discussions

3.1. Surface damage and spalling tendency

Fig. 3 shows the colour change and surface texture of the prismatic specimens of M1 mix. All other mixes also underwent similar colour variation as M1. Both prism and dogbone specimens did not have any apparent major cracks at any of the temperature ranges. Water evaporation can be seen in the form of wide lines on the surface of prisms. Black spots were further noticed on specimens exposed to 600 °C, likely resulting from residue formed by the decomposition of PE fibres present inside the specimen.

It should further be noted that no spalling was observed in any of the mix. These observations are in disagreement with the findings of Li et al. (Li et al., 2020) who reported spalling in the ultra-high performance concrete (1 % PE + 2 % steel) prismatic specimens at 600 °C under similar testing condition (in terms of specimen size and heating rate). This may have been due to the use of silica fume as the main SCM and lower amount of PE fibre content in their study. Therefore, it can be inferred that hybridisation of PE and steel fibre cannot be regarded as ineffective for high-temperature applications. If an optimized fibre volume is paired with the right matrix type, this fibre combination may be useful in spalling prevention. Present study utilizes PE fibre volume of 1.25–1.5 % which has been found effective in resisting spalling till 600 °C exposure in both dogbone and prismatic specimens. However, it is important to note that this behaviour may change if the testing parameters such as heating rate, dwell duration are varied. Rawat et al. (Rawat et al., 2022) observed the matrix containing silica fume and low amount of PE fibre was more prone to spalling at higher heating rates. Therefore, future studies may consider the interaction of these parameters to thoroughly investigate the optimum fibre ratio and matrix proportions.

3.2. Tensile behaviour of HSECC

3.2.1. Stress- strain response

a. Room temperature.

Fig. 4 shows the uniaxial tensile stress–strain curve of HSECC mixes at room temperature. The stress–strain curve of the control specimens underwent three stages: (a) initial elastic stage; (b) strain hardening stage when the specimens undergo multiple fine microcracks; and (c) strain softening stage due to the localisation of failure at one of the cracks. The peak tensile stress was in the range of 10–12 MPa with the highest being for M3 mix. If the mix constituents are compared, M1 and M3 had all similar constituents except the fibre ratio. M3 had higher amount of steel fibres which may have led to relatively higher tensile strength, but lower tensile strain capacity. Mix M4 with only GGBFS as the main binder also showed relatively less ultimate strain capacity, however, this can be further improved significantly with the addition of blends of fly ash and dolomite (M1-M2). Nevertheless, pseudo strain hardening behaviour can be clearly observed in all types of mixes with the value of ultimate tensile strain reaching above 2 % for all cases. This value of ultimate tensile strain is sufficient for use in structural applications (Khan et al., 2020). Moreover, it should further be noted that the designed mixes not only exhibit high strength (compressive strength > 135 MPa, tensile strength > 10 MPa) but also high tensile ductility (ultimate tensile strain > 2 %), ensuring the resilience of critical structures under extreme loads or displacements. The high strength resulted from selecting right matrix constituents at a low water-binder ratio, promoting a densely packed and homogeneous matrix, whereas the high tensile ductility was achieved by appropriate matrix and fibre selection that satisfied micromechanics-based criteria (Ranade et al., 2013) and resulted in strain hardening behaviour as shown in Fig. 4.

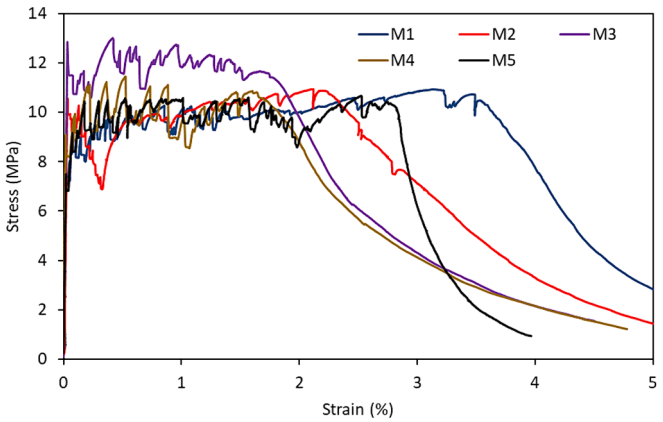

Fig. 4. Tensile stress–strain behaviour of M1-M5 HSECC specimens at room temperature.

Fig. 3. Surface characteristics of M1 mix prismatic specimens on exposure to 20–600 °C.

b. Elevated temperature.

Uniaxial tensile tests were further conducted on all HSECC specimens after exposure to elevated temperature within the selected range and the stress–strain behaviour was recorded. Fig. 5 shows the typical stress–strain behaviour of the HSECC mixes at different temperature ranges.

On increasing the temperature to 200 °C, the strain hardening behaviour was lost and the tensile strength also reduced drastically. This may have been due to the melting of PE fibres which are majorly responsible for the strain hardening behaviour. Moreover, evaporation of free water and loss of cohesion between the CSH layers may also have contributed to this loss in strength. This can further be visualised from the DIC analysis of the tested specimens. The control specimens can be seen to have multiple fine microcracks as observed from Fig. 6a, whereas the 200 °C exposed specimens failed in single crack mainly as a result of the melting of PE fibres (Fig. 6b).

On further increase in the temperature to 400 °C, the tensile strength recovered to a small extent and strain softening behaviour can be observed especially till 400 °C. Even after the initiation of single crack and its propagation, the friction bond between the steel fibre and matrix was large enough to carry the tensile load and therefore, the strain softening behaviour continued. Beyond 500 °C, HSECC lost its strain

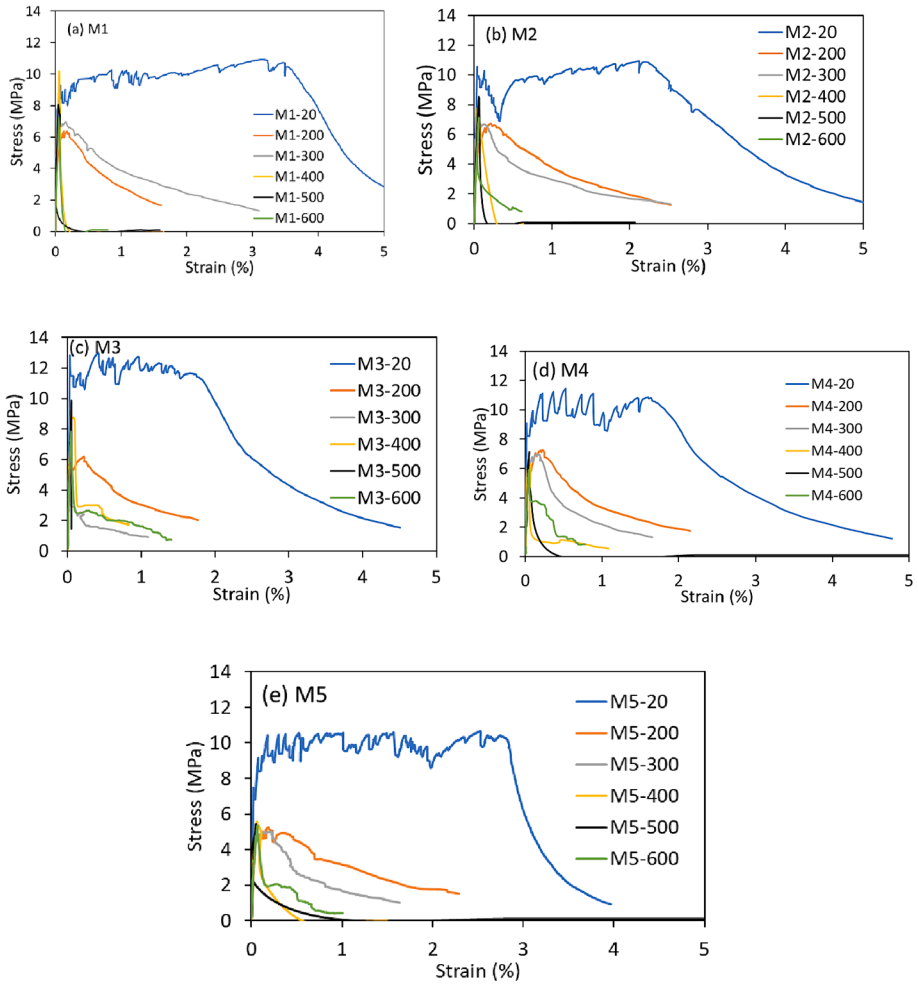

Fig. 5. Tensile stress–strain behaviour of M1-M5 HSECC specimens at different temperatures.

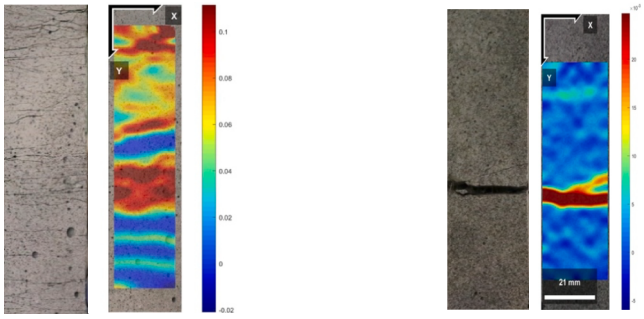

Fig. 6. DIC analysis showing crack pattern in control and 200 °C M1 dog-bone specimens.

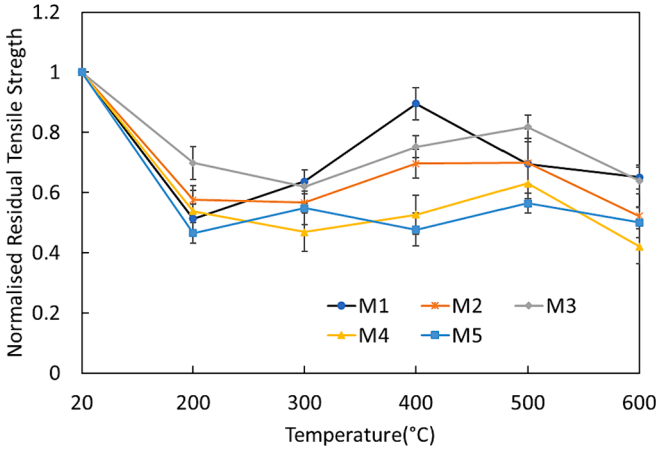

Fig. 7. Normalised residual tensile strength of M1-M5 HSECC specimens at elevated temperatures.

softening behaviour and brittle failure was observed in all types of mixes. At this temperature, the interface bond between the steel fibre and matrix was too small to carry any tensile load and therefore, the softening behaviour was lost.

3.2.2. *Peak tensile stress*

Fig. 7 shows the effect of temperature exposure on the peak tensile stress of HSECC specimens. It can be observed that on increasing the temperature from 20 to 200 °C, the peak tensile stress drastically reduces. A reduction of 30–53 % was observed with M3 showing the least reduction and M5 showing the highest. With further increase in temperature, the peak tensile stress slightly increases up to 400 °C. This could be attributed to an enhanced bond between the matrix and steel fibres within this temperature range. It is possible that improvement in the hydration of CSH occurs till this temperature due to the pozzolanic reaction, as indicated by Lai et al. (Lai et al., 2022) through X-ray diffraction analysis, which may further contribute to a better bond

between the matrix and fibre. This trend was consistently observed for all five mix types where the peak stress either improved or remained at the same level until 400 °C. The maximum rise was observed in M1 with peak stress increased from 51.31 % at 200 °C to 89.52 % at 400 °C. Beyond this temperature, the bond between the steel fibre and matrix deteriorates, leading to a loss in tensile strength. This may be attributed to the continued deterioration of hydration products such as ettringite and portlandite, both of which are likely to decompose by 600 °C (Huang et al., 2024; Huang et al., 2023; Lai et al., 2023). Peak tensile stress reduced to around 42.07–65.08 % at 600 °C with the maximum reduction observed for mix M4 and minimum for mix M1.

Both mix M4 with GGBFS and M5 with silica fume showed a relatively higher reduction in strength with increase at temperature. Mix containing silica fume has higher rate of degradation at elevated temperature due to the densified microstructure of the matrix, making it difficult to control the damage associated with pore pressure. This performance was found to significantly improve with the addition of dolomite powder and fly ash (M1-M2), and this further enhanced with increase in the dolomite content (mix M1) at a constant GGBFS to fly ash ratio. Both fly ash and dolomite powder are beneficial against elevated temperatures. Fly ash-based composites facilitate the formation of tobermorite at elevated temperatures due to accelerated hydration, potentially enhancing strength (Magalhães et al., 2015). In addition, dolomite is decomposed to calcium carbonate and calcium oxide at 315 °C and 528 °C respectively with an additionally generated CO_2 (Olszak-Humienik and Jablonski, 2014). This CO_2 may help resist temperature rise within the internal cross-section (Fauzi et al., 2022), while the resulting calcium carbonate from decomposition may act as a filler, aiding in retention of residual strength. This underscores that, even at the same fibre content, selecting the appropriate binder system such as quaternary blend of GGBFS with fly ash and dolomite can significantly improve the residual strength.

3.2.3. First cracking stress

First cracking stress is defined as the stress corresponding to the appearance of the first stress-drop in the curve which is also the stage of the onset of micro-cracking in HSECC. The initiation of first crack needed relatively high external load due to the associated high toughness of matrix of all types of HSECC as shown in Fig. 8. Fig. 9a further shows a relative comparison of the first cracking stress with the peak stress at room temperature. It can be observed that the first cracking stress was higher than 8 MPa for all mix types with the maximum being for M3 mix. This value is sufficiently high to satisfy the serviceability criteria of structures. On increase in the temperature to 200 °C, the cracking stress also suffered significant decrease of around 48–59 % and followed similar trend as observed for the peak tensile stress. The first cracking stress slightly improved at 300 °C as shown in Fig. 9b. After this temperature, the failure in HSECC mixes was through the localisation of single crack and therefore, the range of peak tensile stress and first cracking stress was similar.

3.2.4. Ultimate tensile strain

Fig. 10 shows the influence of temperature on the ultimate tensile strain of different HSECC mixes. The average ultimate tensile strain at room temperature ranged from 2.12 to 3.67 % with mix M5 showing the highest ductility. On increase in temperature from 20 to 200 °C, the

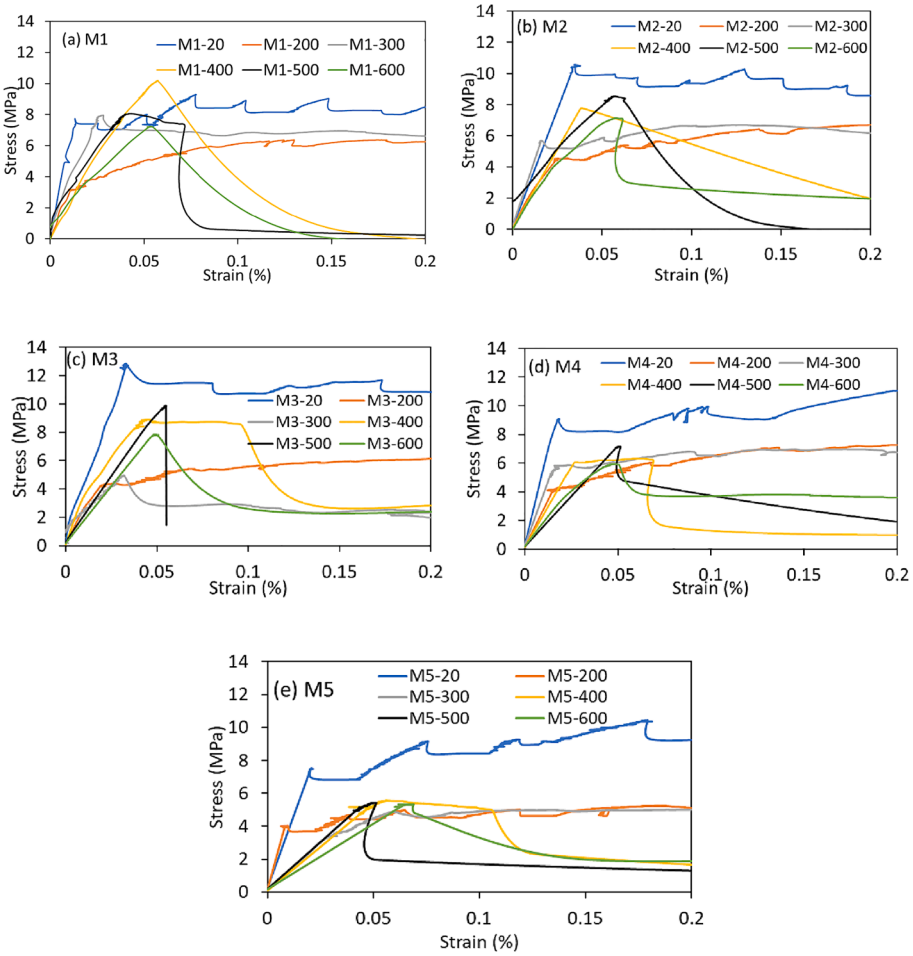

Fig. 8. Tensile stress–strain behaviour of M1-M5 HSECC specimens at different temperature (0–0.2% strain).

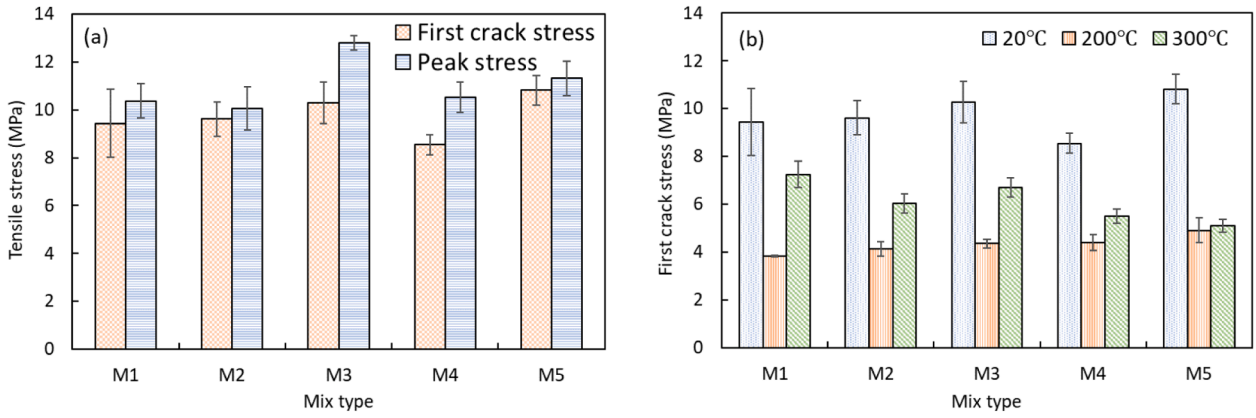

(a) Room temperature peak stress vs first crack stress (b) First crack stress

Fig. 9. First cracking stress of M1-M5 HSECC specimens.

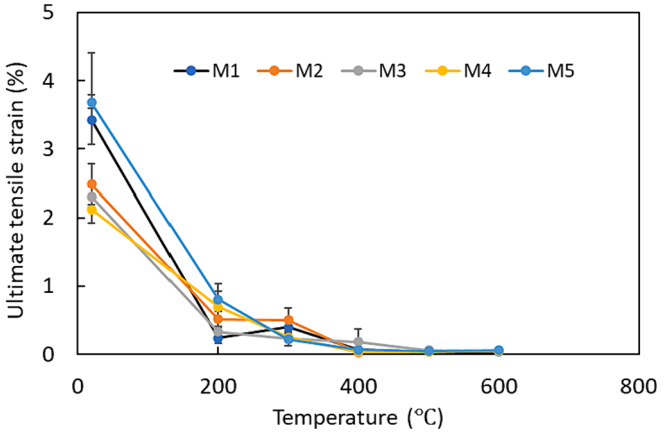

Fig. 10. Ultimate tensile strain of M1-M5 HSECC specimens at elevated temperatures.

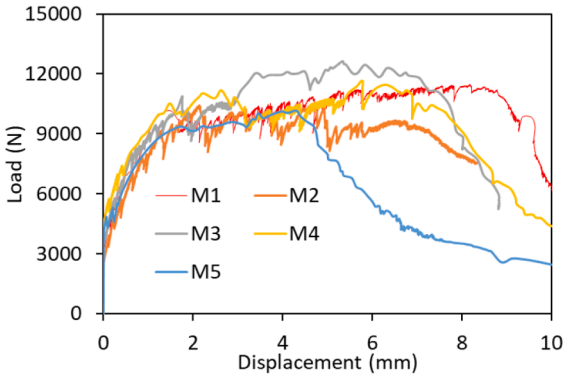

Fig. 11. Load-displacement diagram of control M1-M5 HSECC specimens.

tensile strain capacity reduces drastically to around 0.3–0.8 % due to the melting of PE fibres. At 300 °C, a slight increase in strain capacity was observed, however, it remained much lower than at the control temperature. The ultimate tensile strain was considerably higher at room temperature due to the multiple fine cracking failure mode. With increase in temperature, the intensity of development of multiple fine cracks decreased and specimens failed in a single crack mode. It is interesting to note that the specimens retained a small tensile strain capacity until 300 °C and thereafter, the ultimate strain becomes negligible and quasi-brittle fracture was observed. Due to the little contribution of steel fibre to hardening behaviour, the behaviour after the melting of PE fibre softened and therefore, a continuous reduction in the ultimate tensile strain took place eventually leading to almost negligible strain capacity.

3.3. Flexural behaviour of HSECC

3.3.1. Load-deflection response

a) Room temperature.

The load–deflection curves of M1–M5 HSECC mixes are shown in Fig. 11. It can be seen that all the specimens show flexural hardening behaviour confirming the observations of the tensile tests. The peak flexural load remained in the range of 10–12.5 kN (flexural strength 25.8–28.8 MPa) with the maximum load being observed for M3 mix and minimum for M5 mix. However, the flexural hardening behaviour was more pronounced in the M1 mix as compared to M3 due to higher volume of PE fibres. The overall load–deflection response is similar to the tensile behaviour observed at room temperature.

b) Elevated temperature.

Fig. 12 shows the load displacement curves of M1-M5 specimens after exposure to 20–600 °C. It can be clearly observed that elevated temperature exposure significantly reduces the flexural hardening behaviour. The peak load and hardening behaviour reduce drastically on initial exposure to 200 °C. This initial decrease is generally attributed to the weakening cohesion of Van der Waals forces between the CSH layers. Consequently, the surface energy of the CSH layers decreases, leading to the formation of silanol groups with weaker bond strength (Dawood et al., 2020). Moreover, the melting of PE fibre also contributed significantly to this sudden loss in peak load. The drastic reduction at 200 °C was also observed in the M3 which contained relatively lesser amount of PE fibres. This indicates that the matrix constituents and melting of fibres both contribute to the decrease in the peak flexural load. This can further be visualised from the DIC analysis of the tested specimens. The control specimens can be seen to have multiple fine microcracks as observed from Fig. 13a, whereas the 200 °C exposed specimens did not have any apparent fine cracks and failed by localisation of a single crack after reaching the peak (Fig. 13b).

After 200 °C, the pseudo deflection hardening behaviour and peak flexural load slightly improved as the matrix recovers again with accelerated hydration leading to a better cohesion between the CSH layers and between the fibre and matrix. This effect was consistently

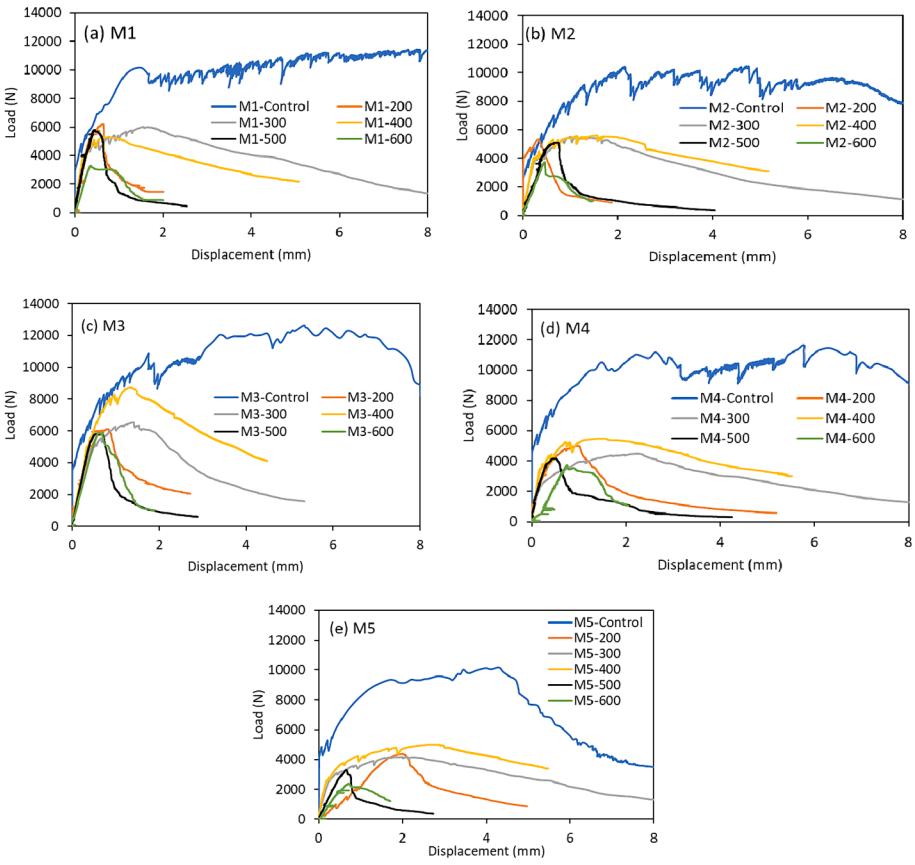

Fig. 12. Load-displacement diagram of M1-M5 HSECC specimens at elevated temperatures.

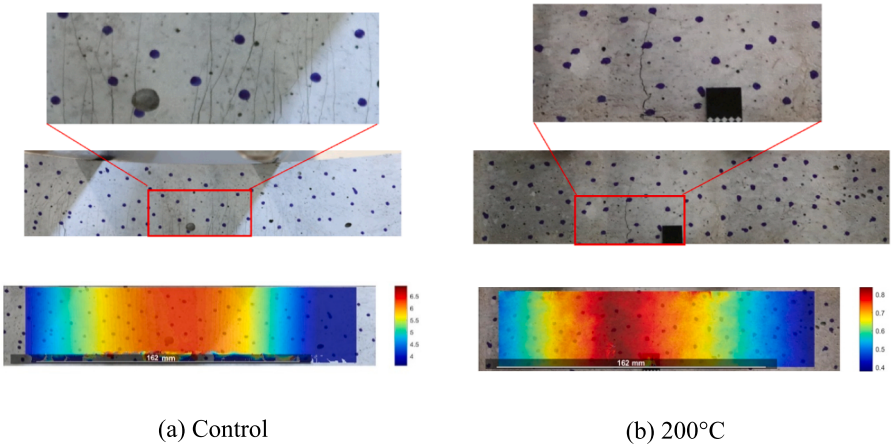

Fig. 13. DIC analysis showing cracking in control and 200 °C exposed M1 prism specimens.

observed for all the mix types. The improvement in the range of 200–400 °C was quite significant for mix M3 which contained higher amount of steel fibres than the rest of the mixes. Not only this mix showed higher peak flexural load, but also an improved pseudo hardening behaviour was observed till 400 °C. On further increase in temperature, the peak load decreased with mix M3 showing the highest retention as expected. The melting point of steel fibres is significantly high than the exposure temperature range. Therefore, a relatively higher load can be resisted by the mix M3 in comparison to other mixes which had low percentage of steel fibres.

3.3.2. *Peak flexural load/strength*

Fig. 14 shows the variation of the average residual peak flexural load with temperature for all five types of mixes. It can be observed that the peak load for M3 was highest at all temperature ranges indicating the positive effect of steel fibres at elevated temperatures after the melting of PE fibres. On increase in the temperature to 200 °C, the residual peak load of M3 reduced drastically with around 61 % retention. This reduction was more severe in other types of mixes with only around 45–50 % retention of peak load at 200 °C. The sudden drop in flexural load may have been due to the melting of PE fibres which contributed to the hardening behaviour and higher peak flexural load at room temperature.

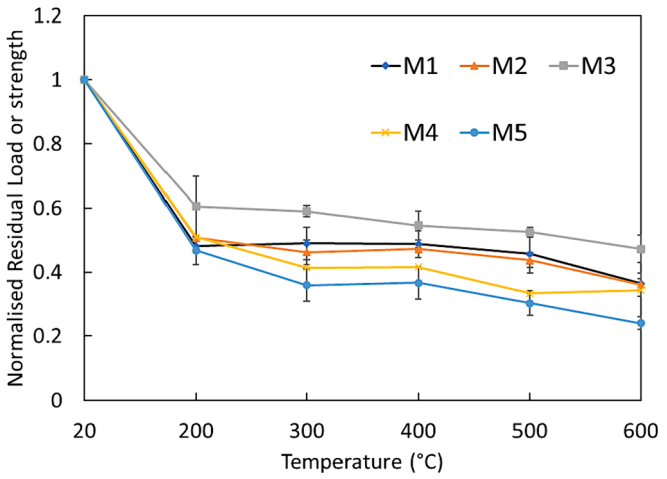

Fig. 14. Normalised peak flexural load/strength of M1-M5 HSECC specimens at elevated temperatures.

All types of mixes had gradual decline in the peak flexural load after 200 °C. The rate of decrease was much slower for mix M3 with approximately 47 % retention at 600 °C. Mix with GGBFS or primary blends of GGBFS and dolomite showed load retention of around 34.3–36.5 % at 600 °C, whereas it was only 24.02 % for M5. In general, mix M5 showed the worst performance among all mixes which may have been due to the higher rate of degradation of matrix consisting of silica fume. Furthermore, it is evident that the performance of GGBFS-based Mix M4 could be enhanced by incorporating blends of dolomite and fly ash (mix M1-M2) due to their beneficial effects as described previously.

3.3.3. *Toughness and toughness index*

a. Room temperature.

Toughness is used to describe the energy absorption capacity of the specimen and is defined as the area under the load–deflection curve upto a specified deflection. The energy absorption capacity of the HSECC mixes is compared as per ASTM C1018 (Astm c1018, 1997) guidelines. The toughness value of the control samples is analysed at four deflections L'/600, L'/150, L'/100 and L'/75, where L' is the effective length of the prism. These values are obtained from the typical load–deflection curve (Fig. 11). Fig. 15 shows the toughness values of M1 to M5 at different deflections. It can be observed that the toughness followed same patterns for all types of mixes with values ranging in similar range. The toughness value of mix M3 with higher steel fibre content was greater than all other mixes indicating that increasing the PE fibre amount may not necessarily lead to increase in the toughness. This may have been due to the increased entrapped air voids and splitting cracks due to the presence of PE fibres (Li et al., 2020). However, this is equally dependent on the matrix type. For instance, the toughness value for M3 was 40.93 Nm at L'/75 deflection, whereas it was 35.89 Nm for M1. Since the only difference in these mixes was that of fibre volume, the variation in toughness can be attributed to the higher amount of PE fibres in M1. However, for mix M4, the toughness value was 38.26 Nm which is closer to M3 in spite of having higher amount of PE fibre indicating that both matrix and fibre are critical for improving the toughness.

Furthermore, toughness index is also compared for control specimens which is used to describe the ductility and is defined as the ratio of the area under the load–deflection curve upto a specified deflection to the area upto the deflection at the first-crack load 'δ.' In general, flexural hardening behaviour can be confirmed if the material possesses toughness index $I_i > i$, where i = 5, 10, 20, 30 (Naaman and Reinhardt, 1996). I_5, I_{10}, I_{20}, and I_{30} are toughness index at deflections 3δ, 5.5 δ, 10.5 δ and 15.5 δ respectively where δ is the deflection at the first crack load. It can be seen from Fig. 16 that the value of toughness index I_i for mix M1 and M5 are close to or greater than the value of i at all the considered deflection range. M2, M3 and M4 shows relatively lower toughness index and hence, does not pass the flexural hardening tests as per the abovementioned criteria. This could be further related to the basic design theory of engineered cementitious composites whereby the tensile strength of the composite must be lower than the fibre bridging strength and the matrix toughness must be low to allow multiple cracking behaviour. With the decrease in PE fibre content or increase in the GGBFS ratio, the overall toughness of the matrix may increase disfavouring the phenomenon of multiple cracking and hence, the toughness index was observed to be lower. The mix M5 containing only silica fume also showed better strain hardening properties in general as it allows the formation of multiple cracks which may have been the reason of its preference by the existing researchers. It is interesting to note that the mix M1 also passes the flexural hardening criteria confirming the possibility of achieving flexural hardening behaviour with a new binder system of dolomite and GGBFS.

b. Elevated temperature.

Fig. 17 further shows the toughness values of HSECC mixes on exposure to elevated temperature at L'/600 and L'/150 deflection. Toughness value for mix M2, M3 and M5 are not reported at L'/150 deflection as the test stopped before reaching that range. Similar to the reduction observed in flexural hardening behaviour, toughness also reduces on increasing the temperature. The toughness of M1 at L'/600 reduced to 38.38 % of the control value at 200 °C. With further increase in temperature, it slightly improved as shown in Fig. 17a and eventually decreased by 64.81 % at 600 °C. This trend was also observed for the toughness values at L'/150 deflection (Fig. 17b). Toughness value for

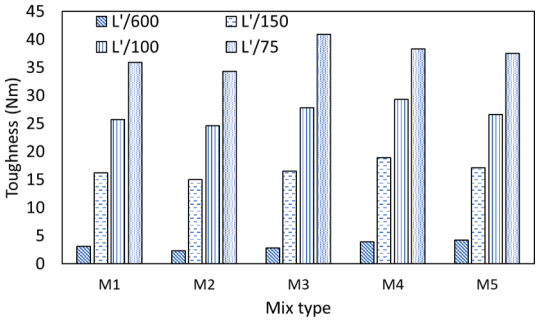

Fig. 15. Toughness of control HSECC specimens at different location.

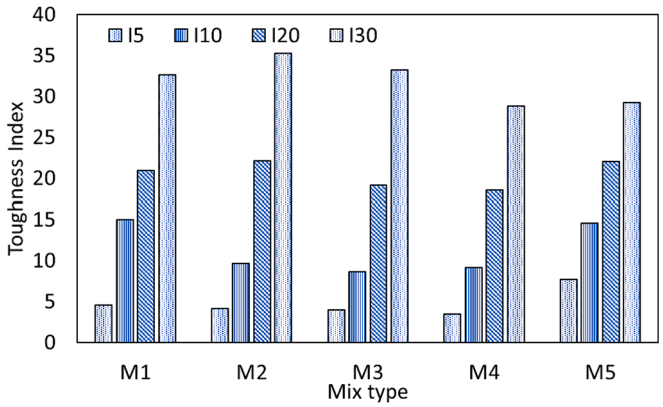

Fig. 16. Toughness index of control M1-M5 HSECC specimens.

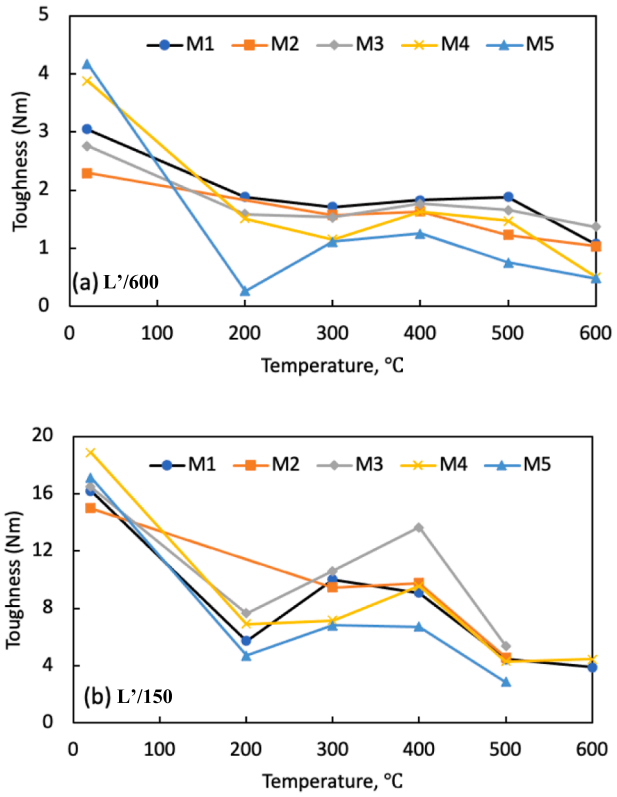

Fig. 17. Toughness of M1-M5 HSECC specimens at elevated temperatures.

M1 at L'/150 deflection reduced by 76.06 % at 600 °C. This behaviour was consistently observed for all other mixes and a slight improvement in the toughness was observed on increasing the temperature from 200 to 400 °C. The maximum reduction in the toughness was observed for M5 mix for which it reduced by 88.42 % at L'/600 deflection at 600 °C and 83.40 % at L'/150 deflection at 500 °C. Overall, the toughness value significantly drops after exposure to elevated temperatures, and this may have been due to the melting of PE fibres and loss of bond between HSECC matrix and steel fibres.

4. Mechanism of fibre degradation at elevated temperatures

Fibres play the most critical role in affecting the uniaxial tensile and flexural properties of HSECC specimens at elevated temperatures and therefore, the physical state of fibres at different temperatures can help in understanding the general behaviour observed through mechanical testing. Consequently, both PE and steel fibres were exposed to 100–800 °C following the same heating profile as mentioned in section 2.3 to analyse stage of fibre degradation. Fig. 18 shows the state of PE and steel fibres at different temperature exposure.

On increasing the temperature from room temperature to 100 °C, no specific change was observed in the physical state of both PE and steel fibres. At 200 °C, PE fibre completely melted, whereas steel fibre did not undergo any noticeable change. This can further be observed from the differential scanning calorimetry (DSC) curve which shows phase change at 150 °C confirming the melting point of PE fibre (Fig. 19a). PE fibres get transformed into a viscous fluid state at this temperature which turns to a solid state on cooling. From 300 to 400 °C, the melted PE fibre further decomposed into a black carbon compound. Steel fibres did not undergo any change in the physical state until 400 °C. On increasing the temperature to 500 °C, PE fibres completely vaporised whereas steel fibres lost its coating and changed to dark grey colour. Thermo-gravimetric (TG) analysis curve also confirmed complete loss of mass of PE fibre at 495 °C. With further increase in the temperature, though there was no difference in the physical state and mass of the steel fibre as confirmed from the TG curve (Fig. 19b), the steel fibres noticeably weakened especially beyond 600 °C.

The same observations can further be confirmed through the SEM images of the M2 HSECC specimens at different temperature ranges (Fig. 20). At 20 °C, PE fibres can be seen suitably bonded with the matrix. With increase in temperature to 200 °C, PE fibres melt leaving a black residue in the fibre channels. This stage continues till 400 °C with the residue still partially visible. After this temperature, the vacant channels can be noticed free from the fibre residues being fully effective for moisture migration. This confirms that PE fibres may have definite role in spalling prevention especially beyond 400 °C. The melting of PE fibres can create clear vacant channels as shown in Fig. 20(d), reducing thermal stress, and potentially preventing spalling or performance degradation. However, below this temperature, the hybrid combination of PE and steel fibres and a suitable thermally better performing matrix is required for better residual performance and spalling resistance.

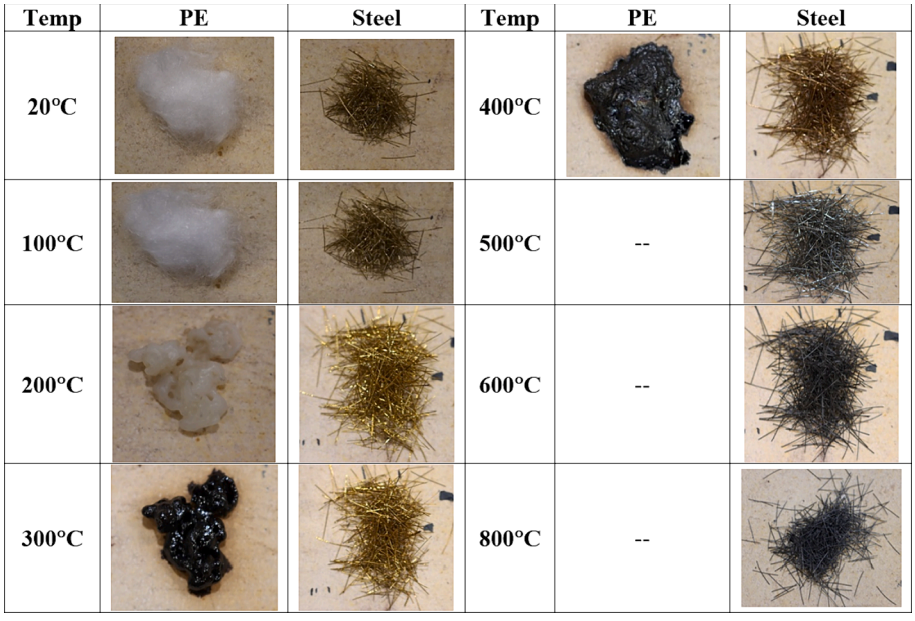

Fig. 18. State of PE and steel fibres at different temperature exposure.

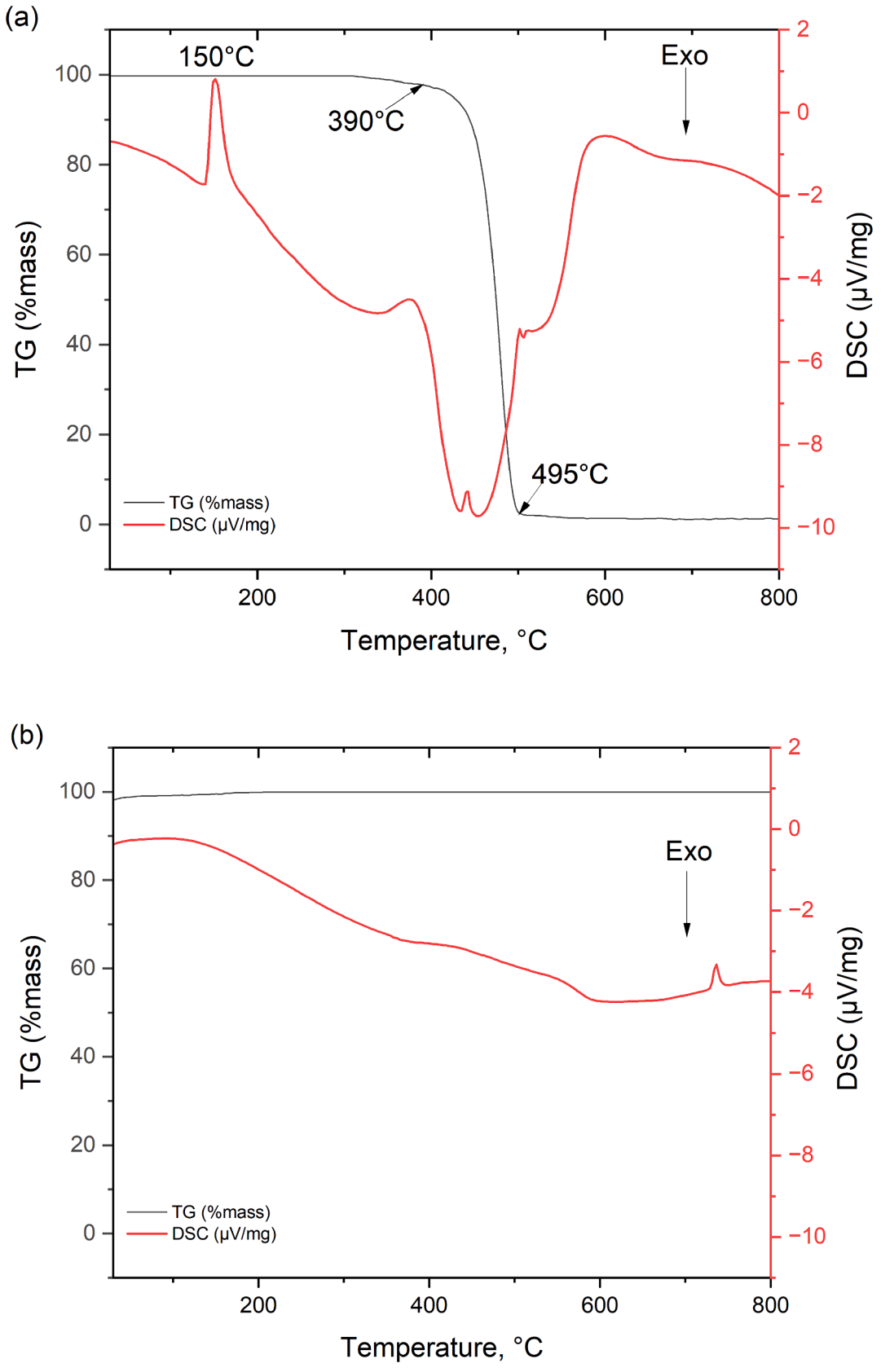

Fig. 19. TG/DSC curve of (a) PE fibre; (b) steel fibre.

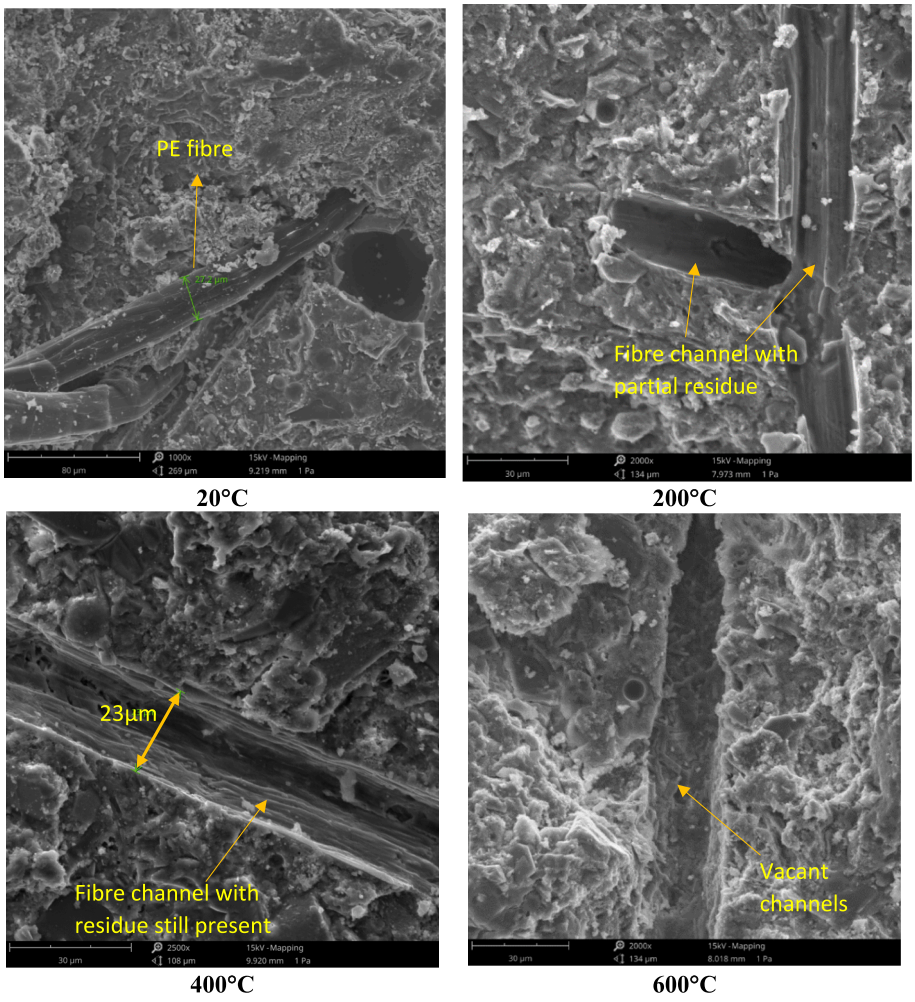

Fig. 20. SEM images of M2 HSECC specimen showing decomposition stages of PE fibre at different temperatures.

5. Conclusions

Present study focused on experimentally investigating the tensile and flexural performance of five different types of hybrid PE-steel fibre based HSECC mixes with different content of SCM and fibre ratio at elevated temperatures. A series of tests including uniaxial tensile, four-point bending, and SEM analysis were conducted to explore the residual properties of HSECC and subsequent stages of fibre degradation at elevated temperatures. Based on the observations, the following conclusions can be drawn.

- It is possible to formulate an HSECC mix with remarkably high cement replacement ratio of upto 60 % without compromising its room temperature and elevated temperature performance. Mix M1 with quaternary blend of GGBFS, fly ash (GGBFS:flyash = 1:0.2) and dolomite powder (15 % by weight) showed the best residual tensile and flexural performance among all HSECC mixes. This performance was also considerably superior to the conventional silica fume mix M5 considered in the study.
- Tensile strength of the mixes reduced substantially with increase in temperatures. There was a sudden decrease initially at 200 °C and thereafter the performance slightly improved at least up to 400 °C. Mix M1 containing dolomite and GGBFS as the main SCM and 1.5 % PE + 0.75 % steel showed the best performance with only 42.07 % reduction at 600 °C. Performance of mix M3 with 1.25 % PE + 1 % steel fibre was also comparable to M1.
- All mixes (M1-M5) showed tensile strain hardening behaviour and flexural hardening at room temperature. The ultimate tensile capacity was found to be more than 2 % confirming the suitability of the considered mixes in structural applications. Pseudo-hardening behaviour was lost on increasing the temperature ($\geq$ 200 °C) due to the melting of PE fibre and the specimens failed due to the localisation of single crack irrespective of the steel fibre content.
- Mix with only GGBFS (M4) or silica fume (M5) showed relatively inferior performance under both tension and flexure than mix with blends of GGBFS, fly ash and dolomite (M1-M3). If considered throughout the temperature rise, mix M5 with silica fume showed the worst performance having a reduction of approximately 45–50 % in the peak tensile stress and around 75 % in peak flexural load at 600 °C. This further confirms the importance of binder selection while targeting high performance at elevated temperatures.
- No spalling was observed in any of the mix irrespective of the volume of the fibres or the matrix constituents. Though complete melting of PE fibres does not take place until 500 °C, necessary spalling resistance can be provided through a synergistic effect of steel and PE fibres and use of appropriate binder system as shown in this study. Nevertheless, focus should also be kept on the right selection of binder material and use of silica fume should be minimized for attaining greater residual performance.

CRediT authorship contribution statement

S. Rawat: Writing – original draft, Validation, Methodology,

Investigation, Formal analysis, Data curation, Conceptualization. **C.K. Lee:** Writing – review & editing, Supervision, Resources, Project administration, Methodology, Conceptualization. **Y.X. Zhang:** Writing – review & editing, Supervision, Resources, Methodology, Funding acquisition, Conceptualization.

Declaration of competing interest

The authors declare that they have no known competing financial interests or personal relationships that could have appeared to influence the work reported in this paper.

Data availability

Data will be made available on request.

Acknowledgment

Commonwealth's support for this research received through Australian Government RTP and UNSW Canberra's support through UIPA Scholarship are gratefully acknowledged. Sponsoring of HRWR by GCP Applied Technologies, Australia, and dune sand by Holcim Quarries, Bungendore is gratefully acknowledged. Support from ARC Discovery Project [DP220103043] is also acknowledged. The authors would also like to thank Dr Daniel J. Fanna, Dr Laurel George, and Dr Richard Wuhrer from Advanced Materials Characterisation Facility (AMCF), Western Sydney University for access to instrumentation and training.

References

Amran, M., Murali, G., Khalid, N.H.A., Fediuk, R., Ozbakkaloglu, T., Lee, Y.H., Haruna, S., Lee, Y.Y., 2021. Slag uses in making an ecofriendly and sustainable concrete: a review. Constr. Build. Mater. 272, 121942 https://doi.org/10.1016/j.conbuildmat.2020.121942.

Astm c1018,, 1997. Standard test method for flexural toughness and first-Crack strength of fiber-reinforced concrete (using beam with third-point loading). ASTM International.

Astm c1609,, 2019. Standard test method for flexural performance of fiber-reinforced concrete (using beam with third-point loading). ASTM International.

Dawood, E.T., Alattar, A.A., Abbas, W.A., Mohammad, Y.Z., 2020. Behavior of foamed concrete reinforced with hybrid fibers and exposed to elevated temperatures. SN Applied Sciences 2 (1), 84. https://doi.org/10.1007/s42452-019-1856-7.

Deng, Y., Yan, C., Zhang, J., Yin, L., Liu, S., Yan, Y., 2022. Preparation and mechanical characterization of engineered cementitious composites with high-volume fly ash and waste glass powder. J. Clean. Prod. 333, 130222 https://doi.org/10.1016/j.jclepro.2021.130222.

Fauzi, A., Amalia, A., Osman, A.F., Alrashdi, A.A., Mustafa, Z., Halim, K.A.A., 2022. On the use of dolomite as a mineral filler and co-filler in the field of polymer composites: a review. Polymers 14, 2843. https://doi.org/10.3390/polym14142843.

Ho, J.C.M., Liang, Y., Wang, Y.H., Lai, M.H., Huang, Z.C., Yang, D., Zhang, Q.L., 2022. Residual properties of steel slag coarse aggregate concrete after exposure to elevated temperatures. Constr. Build. Mater. 316, 125751 https://doi.org/10.1016/j.conbuildmat.2021.125751.

Hou, M., Zhang, D., Li, V.C., 2022. Material processing, microstructure, and composite properties of low carbon engineered cementitious composites (ECC). Cem. Concr. Compos. 134, 104790 https://doi.org/10.1016/j.cemconcomp.2022.104790.

Huang, Z.C., Liu, J.J., Ren, F.M., Cui, J., Song, Z., Lu, D.H., Lai, M.H. Behavior of SSFA high-strength concrete at ambient and after exposure to elevated temperatures, Case Studies in Construction Materials (2024) e02946. https://doi.org/10.1016/j.cscm.2024.e02946.

Huang, Z.C., Ho, J.C.M., Cui, J., Ren, F.M., Cheng, X., Lai, M.H., 2023. Improving the post-fire behaviour of steel slag coarse aggregate concrete by adding GGBFS. Journal of Building Engineering 76, 107283. https://doi.org/10.1016/j.jobe.2023.107283.

Khan, M.K.I., Zhang, Y.X., Lee, C.K., 2020. Mechanical properties of high-strength steel–polyvinyl alcohol hybrid fibre engineered cementitious composites. J. Struct. Integrity Maint. 6 (1), 47–57. https://doi.org/10.1080/24705314.2020.1823558.

Lai, M.H., Binhowimal, S.A.M., Griffith, A.M., Hanzic, L., Wang, Q., Chen, Z., Ho, J.C.M., 2021. Shrinkage design model of concrete incorporating wet packing density. Constr. Build. Mater. 280, 122448 https://doi.org/10.1016/j.conbuildmat.2021.122448.

Lai, M.H., Huang, Z.C., Wang, C.T., Wang, Y.H., Chen, L.J., Ho, J.C.M., 2022. Effect of fillers on the behaviour of low carbon footprint concrete at and after exposure to elevated temperatures. Journal of Building Engineering 51, 104117. https://doi.org/10.1016/j.jobe.2022.104117.

Lai, M.H., Binhowimal, S.A.M., Griffith, A.M., Hanzic, L., Chen, Z., Wang, Q., Ho, J.C.M., 2022. Shrinkage, cementitious paste volume, and wet packing density of concrete. Struct. Concr. 23 (1), 488–504. https://doi.org/10.1002/suco.202000407.

Lai, M.H., Chen, Z.H., Cui, J., Zhong, J.P., Wu, Z.R., Ho, J.C.M., 2023. Enhancing the post-fire behavior of steel slag normal-strength concrete by adding SCM. Constr. Build. Mater. 398, 132336 https://doi.org/10.1016/j.conbuildmat.2023.132336.

Lai, M.H., Lu, Z.Y., Luo, Y.T., Ren, F.M., Cui, J., Wu, Z.R., Ho, J.C.M., 2024. Pre-and post-fire behaviour of glass concrete from wet packing density perspective. Journal of Building Engineering, 108758. https://doi.org/10.1016/j.jobe.2024.108758.

Lao, J.C., Xu, L.Y., Huang, B.T., Dai, J.G., Shah, S.P., 2022. Strain-hardening ultra-high performance geopolymer concrete (UHPGC): matrix design and effect of steel fibers. Compos. Commun. 30, 101081 https://doi.org/10.1016/j.coco.2022.101081.

Lao, J.C., Huang, B.T., Fang, Y., Xu, L.Y., Dai, J.G., Shah, S.P., 2023. Strain-hardening alkali-activated fly ash/slag composites with ultra-high compressive strength and ultra-high tensile ductility. Cem. Concr. Res. 165, 107075 https://doi.org/10.1016/j.cemconres.2022.107075.

Li, Y., Yang, E.H., Tan, K.H., 2020. Flexural behavior of ultra-high performance hybrid fiber reinforced concrete at the ambient and elevated temperature. Constr. Build. Mater. 250, 118487 https://doi.org/10.1016/j.conbuildmat.2020.118487.

Liu, J.C., Tan, K.H., 2018. Fire resistance of ultra-high performance strain hardening cementitious composite: residual mechanical properties and spalling resistance. Cem. Concr. Compos. 89, 62–75. https://doi.org/10.1016/j.cemconcomp.2018.02.014.

Magalhães, M.D.S., Toledo Filho, R.D., Fairbairn, E.D.M.R., 2015. Thermal stability of PVA fiber strain hardening cement-based composites. Constr. Build. Mater. 94, 437–447. https://doi.org/10.1016/j.conbuildmat.2015.07.039.

Meng, D., Huang, T., Zhang, Y.X., Lee, C.K., 2017. Mechanical behaviour of a polyvinyl alcohol fibre reinforced engineered cementitious composite (PVA-ECC) using local ingredients. Constr. Build. Mater. 141, 259–270. https://doi.org/10.1016/j.conbuildmat.2017.02.158.

Mikhailova, O., Yakovlev, G., Maeva, I., Senkov, S., 2013. Effect of dolomite limestone powder on the compressive strength of concrete. Procedia Eng. 57, 775–780. https://doi.org/10.1016/j.proeng.2013.04.098.

Naaman, A., Reinhardt, H.W., 1996. Characterization of high performance fiber reinforced cement composites-HPFRCC. High Performance Fiber Reinforced Cement Composites 2, 1–23.

Olszak-Humienik, M., Jablonski, M., 2014. Thermal behavior of natural dolomite. J. Therm. Anal. Calorim. 119 (3), 2239–2248. https://doi.org/10.1007/s10973-014-4301-6.

Ranade, R., Li, V.C., Stults, M.D., Heard, W.F., Rushing, T.S., 2013. Composite properties of high-strength, high-ductility concrete. ACI Mater. J. 110 (4).

Rawat, S., Zhang, Y.X., Lee, C.K. Spalling resistance of hybrid polyethylene and steel fiber-reinforced high-strength engineered cementitious composite, in: Duan, W., Zhang, L., Shah, S.P. (Eds.) Nanotechnology in Construction for Circular Economy. NICOM 2022. Lecture Notes in Civil Engineering, vol 356. Springer, Singapore. https://doi.org/10.1007/978-981-99-3330-3_33.

Rawat, S., Lee, C.K., Zhang, Y.X., 2021. Performance of fibre-reinforced cementitious composites at elevated temperatures: a review. Constr. Build. Mater. 292, 123382 https://doi.org/10.1016/j.conbuildmat.2021.123382.

Rawat, S., Zhang, Y.X., Lee, C.K., 2022. Multi-response optimization of hybrid fibre engineered cementitious composite using Grey-Taguchi method and utility concept. Constr. Build. Mater. 319, 126040 https://doi.org/10.1016/j.conbuildmat.2021.126040.

Rawat, S., Lee, C.K., Zhang, Y.X., 2024. In-situ compressive and tensile performances of high strength engineered cementitious composite at elevated temperatures. Struct. Concr. https://doi.org/10.1002/suco.202300724.

Shoji, D., He, Z., Zhang, D., Li, V.C., 2022. The greening of engineered cementitious composites (ECC): a review. Constr. Build. Mater. 327, 126701 https://doi.org/10.1016/j.conbuildmat.2022.126701.

Sullivan, P.J.E., Sharshar, R., 1992. The performance of concrete at elevated temperatures (as measured by the reduction in compressive strength). Fire Technol. 28 (3), 240–250. https://doi.org/10.1007/BF01857693.

Tangirala, A., Rawat, S., Lahoti, M., 2023. High volume fly ash and basalt-polypropylene fibres as performance enhancers of novel fire-resistant fibre reinforced cementitious composites. Journal of Building Engineering 78, 107586. https://doi.org/10.1016/j.jobe.2023.107586.

Tosun-Felekoğlu, K., Gödek, E., Keskinateş, M., Felekoğlu, B., 2017. Utilization and selection of proper fly ash in cost effective green HTPP-ECC design. J. Clean. Prod. 149, 557–568. https://doi.org/10.1016/j.jclepro.2017.02.117.

Yang, Z., Xiong, X., Li, K., Briseghella, B., Marano, G.C., Chen, S., 2024. Long-term volume stability of ECC containing high-volume steel slag. Cem. Concr. Compos. 145, 105352 https://doi.org/10.1016/j.cemconcomp.2023.105352.

Yu, J., Wu, H.L., Leung, C.K.Y., 2020. Feasibility of using ultrahigh-volume limestone-calcined clay blend to develop sustainable medium-strength engineered cementitious composites (ECC). J. Clean. Prod. 262, 121343.

Zhang, D., Jaworska, B., He, Z., Dahlquist, K., Li, V.C., 2020. Engineered cementitious composites (ECC) with limestone calcined clay cement (LC3). Cem. Concr. Compos. 114, 103766 https://doi.org/10.1016/j.cemconcomp.2020.103766.

Zhang, Z., Liu, S., Yang, F., Weng, Y., Qian, S., 2021. Sustainable high strength, high ductility engineered cementitious composites (ECC) with substitution of cement by rice husk ash. J. Clean. Prod. 317, 128379 https://doi.org/10.1016/j.jclepro.2021.128379.

Zhang, D., Liu, Y., Tan, K.H., 2021. Spalling resistance and mechanical properties of strain-hardening ultra-high performance concrete at elevated temperature. Constr. Build. Mater. 266, 120961 https://doi.org/10.1016/j.conbuildmat.2020.120961.

Zhang, Z., Yuvaraj, A., Di, J., Qian, S., 2019. Matrix design of light weight, high strength, high ductility ECC. Constr. Build. Mater. 210, 188–197. https://doi.org/10.1016/j.conbuildmat.2019.03.159.

Zhuang, X., Liang, Y., Ho, J.C.M., Wang, Y.H., Lai, M.H., Li, X., Xu, Z., Xu, Y., 2022. Post-fire behavior of steel slag fine aggregate concrete. Struct. Concr. 23 (6), 3672–3695. https://doi.org/10.1002/suco.202100677.